VASCULAR REMODELING OF CHOROIDAL NEOVASCULARIZATION AFTER ANTI–VASCULAR ENDOTHELIAL GROWTH FACTOR THERAPY VISUALIZED ON OPTICAL COHERENCE TOMOGRAPHY ANGIOGRAPHY

ALEXANDRA MIERE, MD,* PAULINE BUTORI, MD,* SALOMON Y. COHEN, MD, PHD,*†
OUDY SEMOUN, MD,* VITTORIO CAPUANO, MD,* CAMILLE JUNG, MD, PHD,†
ERIC H. SOUIED, MD, PHD*†

Purpose: To describe the qualitative and quantitative changes in choroidal neovascularization (CNV) flow pattern after anti–vascular endothelial growth factor therapy, by optical coherence tomography angiography (OCTA).

Methods: Consecutive patients with neovascular age-related macular degeneration underwent multimodal imaging, including OCTA at initial examination and at last visit. High-flow networks in the choriocapillaris segmentation of OCTA were qualitatively and quantitatively analyzed at baseline and at follow-up, to characterize vascular flow changes after anti–vascular endothelial growth factor treatment and to correlate these changes with final exudation signs on spectral domain optical coherence tomography.

Results: Seventeen eyes were included. Mean follow-up was of 11.7 ± 3.3 months. Baseline images showed six medusa pattern (35.3%), four seafan pattern (23.5%), and seven indistinct network patterns (41.2%). Mean CNV area at baseline was 1.58 ± 1.72 mm^2. Final OCTA images revealed a decrease in CNV total area of 21.6%. In 6/17 eyes, the baseline neovascular pattern was unchanged; these cases were associated with exudation at the final spectral domain optical coherence tomography examination (P = 0.034) and a decrease in CNV area of 34.1%. Conversely, in 11/17 eyes (64.7%), the initial pattern had changed to a pruned vascular tree pattern, with variable exudative status on spectral domain optical coherence tomography at the final visit and a decrease in total CNV area of 0.07%.

Conclusion: The vascular flow remodeling induced by recurrent anti–vascular endothelial growth factor treatment can be assessed by OCTA. Optical coherence tomography angiography may help to accurately evaluate treatment response and to recognize patterns usually associated with recurrent exudative activity.

RETINA 0:1–10, 2017

Exudative age-related macular degeneration (AMD) is the first cause of vision impairment in western countries.[1,2] Choroidal neovascularization (CNV) plays a key role in the pathogenesis of AMD. Classically, fluorescein angiography is the gold standard for diagnosing CNV.[3,4] Angiographic features of CNV types associated with neovascular AMD have been extensively described, to clearly delineate between occult CNV (Type 1),[3,5] classic CNV (Type 2),[6] and Type 3 neovascularization (retinoretinal or retinochoroidal anastomosis).[7–9] Staining and leakage on late frames of the fluorescein angiography examination generate essential images for the diagnosis of exudative AMD. However, intravenous fluorescein injection is known to have various side effects, ranging from nausea to anaphylaxis.[10] Thus, the advent of high-resolution optical coherence tomography provided a noninvasive structural imaging technique for patients

with CNV. Currently, spectral domain optical coherence tomography (SD-OCT) is widely used to assess retinal and choroidal abnormalities in macular disease in general and in AMD in particular because it provides fast, noninvasive information on recurrence, and treatment response.[11] On SD-OCT, CNV is characterized by subretinal (Type 2 CNV) or sub-RPE (Type 1 CNV) hyperreflective lesions.[3] However, because of similar reflectivity, a clear differentiation between vascular and fibrous tissue is difficult. Both conventional angiography and SD-OCT generate two-dimensional images, enabling an indirect visualization of the CNV either by late leakage or the presence of subretinal and intraretinal fluid, but the actual location, morphology, and area of the CNV are difficultly evaluated.

By detecting blood flow, optical coherence tomography angiography (OCTA) is a noninvasive, innovative approach in the detection of CNV associated with neovascular AMD. This advanced motion contrast imaging uses amplitude decorrelation technology and high frequency scanning for an in vivo detection of erythrocyte movement (and thus blood flow) inside the retinal and choroidal vasculature.[12–14] Thus, a precise morphologic analysis of CNV flow is now achievable.

Optical coherence tomography angiography findings in Type 1,[15] Type 2,[16] Type 3,[17] and fibrotic CNV[18] associated with neovascular AMD have been described in recent studies. Choroidal neovascularization corresponds almost to a high-flow lesion on OCTA images, with variable sensitivity when compared with multimodal imaging. Although CNV presented with variable morphological features, in some cases, CNV shared a similar microvascular organization. Thus, different patterns were described and named according to specific morphologic features. In Type 1 CNV, Kuehlewein et al[15] described a "medusa" pattern (with vessels radiating in all directions from the center of the lesion), a "seafan" pattern (vessels radiating in all directions from one side of the lesion) and an indistinct pattern. Similar patterns were found in Type 2 CNV by El Ameen et al[16], with a peculiar "seafan" pattern named "glomerulus-shaped" lesion. The study of subretinal fibrosis in OCTA distinguished three other patterns that were described by Miere et al[18] as pruned vascular tree, tangled network, and vascular loop. The relevance of such morphologic descriptions is still debated. One of the questions raised by previous studies is whether one pattern remains the same over time or progresses toward another pattern during the follow-up.

Morphologic changes of neovascular membranes during anti–vascular endothelial growth factor (VEGF) treatment over time are not fully known yet. This study aimed to assess, throughout a long-term follow-up on OCTA, the morphologic changes in different CNV patterns in patients with active CNV secondary to neovascular AMD undergoing anti-VEGF therapy.

Methods

This retrospective monocentric case series included consecutive patients with active Type 1, Type 2, and mixed Type 1 and 2 CNV in AMD, both previously treated and treatment naive, presenting at the University Eye Clinic of Creteil between October 2014 and February 2015. All cases had a minimum follow-up duration of 6 months. Eligibility criteria were a diagnosis of CNV based on the fluorescein angiography international AMD classification,[19] the absence of important media opacities and a correct target fixation, allowing for good quality OCTA images. Exclusion criteria included other forms of neovascular AMD, such as Type 3 neovascularization, idiopathic polypoidal choroidal vasculopathy, ocular diseases associated with pigment epithelial detachments, adult onset foveomacular vitelliform dystrophy, history of highly myopic CNV or pathologic myopia, and a history of inherited macular dystrophies.

At baseline, each patient underwent a complete clinical and paraclinical examination including best-corrected visual acuity (BCVA) measured with the Early Treatment Diabetic Retinopathy Study chart, fundus examination, fluorescein angiography, indocyanine green angiography, SD-OCT (HRA, Heidelberg Engineering, Heidelberg, Germany), and OCTA imaging (AngioVue RTVue XR Avanti; Optovue, Inc, Freemont, CA).

Included patients underwent either fixed or PRN regimens of anti-VEGF treatment. The final examination included BCVA measurement, fundus examination, SD-OCT, and OCTA at least 6 months after the baseline examination.

From the *Department of Ophthalmology, Centre Hospitalier Intercommunal de Créteil, University Paris Est Créteil, Créteil, France; and †Clinical Research Center, GRC Macula, Centre Hospitalier Intercommunal de Créteil, France.

S. Y. Cohen consultant for Alcon (Hünenberg, Switzerland), Allergan Inc (Irvine, CA), Novartis (Basel, Switzerland), Bayer Shering-Pharma (Berlin, Germany), Farmila-Thea (Clermont-Ferrand, France), Roche (San Francisco, CA). O. Semoun consultant for Novartis (Basel, Switzerland), Bayer Shering-Pharma (Berlin, Germany), Allergan Inc (Irvine, CA), Optovue (Freemont, CA). E. H. Souied consultant for consultant for Novartis (Basel, Switzerland), Bayer Shering-Pharma (Berlin, Germany), Allergan Inc (Irvine, CA), Farmila-Thea (Clermont-Ferrand, France). The remaining authors have no financial/conflicting interests to disclose.

Reprint requests: Eric H. Souied, MD, PhD, Department of Ophthalmology, Centre Hospitalier Intercommunal de Créteil, Université de Paris Est Créteil, 40 Avenue de Verdun, Créteil 94000, France; e-mail: eric.souied@chicreteil.fr

Optical coherence tomography angiography is a novel imaging technique using the split-spectrum amplitude-decorrelation angiography algorithm to generate amplitude-decorrelation angiography images. The instrument is designed to obtain amplitude decorrelation angiography images. This instrument has an A scan rate of 70,000 scans per second, using a light source centered on 840 nm and a bandwidth of 50 nm. Each OCTA volume contains 304 × 304 A scans with two consecutive B scans captured at each fixed position before proceeding to the next sampling location. Split-spectrum amplitude-decorrelation angiography was used to extract the OCTA information. Each OCTA volume is acquired in 3 seconds, and 2 orthogonal OCTA volumes were acquired to perform motion correction to minimize motion artifacts arising from microsaccades and fixation changes. Angiography information displayed is the average of the decorrelation values when viewed perpendicularly through the thickness being evaluated. The machine software provides an automatic retinal and choroidal segmentation for image analysis. In our study, the different morphologic patterns of CNV that were previously described in the literature were recognized at baseline and analyzed over time in both outer retina and choriocapillaris automatic segmentations. Moreover, microvascular flow changes were noticed over time, such as enlarged vessels, anastomosis vascular loops, sprouting capillaries, and no flow areas.

For each eye, OCTA was performed using a 3 × 3 scanning area. Baseline OCTA imaging was compared with the final one. Based on recent literature,[15–18,20] two experienced readers (P.B. and A.M.) described the presence or the absence of six specific morphologic features of CNV high-flow networks (in the choriocapillaris segmentation) over time, as follows:

1. A high-flow vascular network;
2. A visible feeder vessel (a larger vessel from where the other vascular trunks seemed to emerge) either at the center or peripheral to the high-flow neovascular membrane;
3. The presence of thin branches (defined as tiny, numerous capillaries sprouting from larger vascular trunks) within the high-flow neovascular lesion;
4. Presence of a circular surrounding anastomosis or of margin loops at the lesion's extremity;
5. Persistence of solely large vascular trunks with filamentous flow and without any secondary ramifications;
6. A dark halo.

These 6 characteristics throughout literature[15–18,20] generated 4 patterns of high-flow, neovascular membranes (Figure 1 and Table 1). First, "medusa" pattern, including a central feeder vessel, circular peripheral anastomosis, thin branches, and a surrounding hypointense halo in the choriocapillaris segmentation.

Second, a "seafan" pattern, harboring a peripheral/eccentric feeder vessel associated with thin branches, a hypointense halo, and no circular peripheral anastomosis. Furthermore "indistinct network" pattern was characterized by no visible feeder vessel, thin branches, and a hypointense halo. Finally, "pruned vascular tree" pattern is defined by a filamentous flow, with persistence of main vascular trunks but no thin ramifications and a variable visualization of a feeder vessel. Moreover, flow void was described in cases presenting a low flow or no flow area, without a discernible high-flow vascular network.

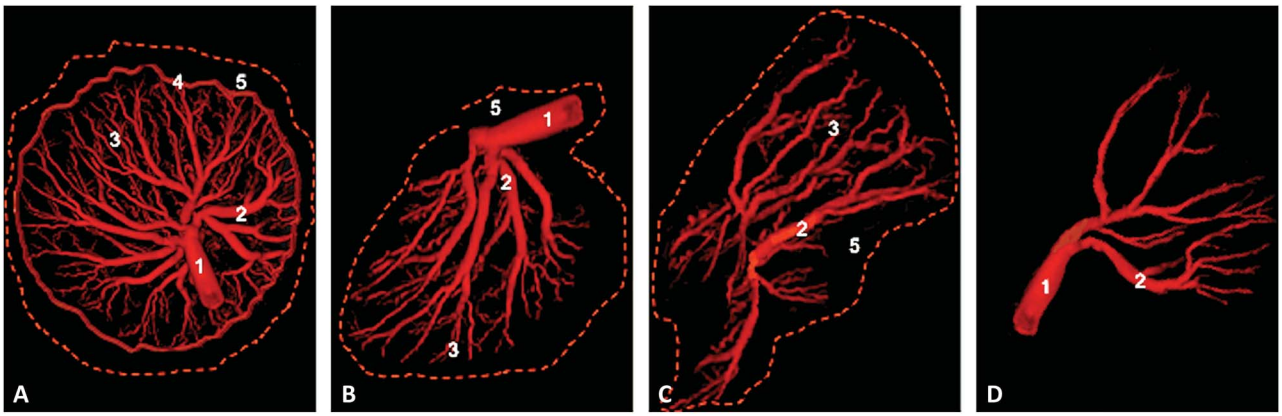

Fig. 1. Illustrative drawing showing different CNV patterns in OCTA. **A.** "Medusa" pattern, consisting of a central feeder vessel (1), centrifugal vascular trunks (2), tiny capillaries (3), and a circular peripheral anastomosis (4). A surrounding dark halo (5) can be observed. **B.** "Seafan" pattern, consisting of an eccentric feeder vessel (1), main vascular trunks (2), tiny capillary ramifications (3), and an optional dark halo (5). **C.** "indistinct network" pattern was characterized by the visualization of only main vascular trunks (2) and thin branches (3) but with no detectable feeder vessel; a dark halo and/or a circumferential peripheral anastomosis may be observed (5). **D.** "pruned vascular tree" pattern is defined by a variable visualization of feeder vessel (1), with persistence of main vascular trunks (2) but no thin ramifications.

Table 1. Characterization of the Four Different Patterns of CNV High-Flow Networks Using Specific Morphologic OCTA Features

	Thin Branches	Circular Peripheral Anastomosis	Feeder Vessel	Filamentous Flow	Dark Halo*
Immature patterns					
Medusa	Yes	Yes†	Yes, central†	No	Yes
Seafan	Yes	No	Yes, peripheral	No	Yes
Indistinct	Yes	No	Not visible	No	Yes
Mature pattern					
Pruned vascular tree	No	No	Yes or no	Yes	Yes or no

*This inconstant feature is not indispensable to classify a high-flow network in an immature pattern.
†One of these two features is sufficient to classify in a medusa pattern.

Images corresponding to the choriocapillaris segmentation of the OCTA, obtained at baseline and at the final visit, were masked and analyzed by two experimented readers (P.B. and A.M.). A senior reader (S.Y.C.) adjudicated contentious cases in both instances. Comparison between the type of pattern and presence/absence of exudation observed on B scans of the optical coherence tomography was also performed.

To measure CNV area on OCTA images, we used the AngioAnalystics System provided by the AngioVue software (AngioVue RTVue XR Avanti; Optovue, Inc, Freemont, CA). The incorporated flow area draw tool allowed a user-defined quantification of vascular area at the automatic choriocapillaris segmentation, followed by an automatic computation or "select area" and "vessel area." "Select area" corresponds to the total area manually measured, whereas "vessel area" corresponds to the total area of vessels with detectable flow within the manually selected total area. For clarity, we will refer to "select area" as "total area."

Statistical analysis was performed using STATA software (version 13.0; StataCorp LP, College Station, TX) and included descriptive statistics for main clinical features. Chi-square or Fisher exact tests were used to compare qualitative variables, and the Wilcoxon test was used to compare quantitative data. To quantify the interuser agreement, a Kappa coefficient was computed. For quantitative variables, interclass correlation and 95% confidence interval were evaluated for lesion measurements between Readers 1 and 2. For all findings, the chosen level of statistical significance was $P < 0.05$. Optical coherence tomography angiography findings at baseline and follow-up were compared with SD-OCT imaging, to establish an association between different patterns and SD-OCT exudative signs.

This study was performed in accordance with the Declaration of Helsinki and current French legislation and with approval of our local ethics committee.

Results

Seventeen eyes from 16 patients with exudative AMD were included. Patients were 4 men and 12 women aged from 68 to 89 years (mean: 81 ± 6.5 years). Type 1 CNV was diagnosed in 5/17 cases (29.4%), Type 2 CNV in 9/17 cases (52.9%), and mixed Type 1 and 2 CNV in 3/17 cases (17.6%). At initial examination, eyes were naive of treatment in 9/17 cases (52.9%), whereas the 8/17 previously treated eyes had received an average of 8.4 ± 5.5 intravitreal injections. The mean duration of follow-up between initial and final examination was 11.7 ± 3.3 months (6–17 months). The initial mean BCVA was 0.38 ± 0.49 logMAR (Snellen equivalent: 20/50). At final examination, all patients had received from an average of 7.3 ± 2.3 intravitreal injections during the follow-up duration. The final mean BCVA was 0.28 ± 0.38 logMAR (Snellen equivalent: 20/40). Demographic and clinical features are described in Table 2.

Changing Patterns Versus Constant Patterns

At baseline, OCTA images depicted seven indistinct network patterns (41.2%) (Figures 1 and 2), six medusa patterns (35.3%) (Figures 1 and 3) and four seafan patterns (23.5%) (Figure 1). Mean total CNV area at baseline was 1.58 ± 1.72 mm^2, whereas vessel area averaged 0.88 ± 0.95 mm^2. Corresponding initial SD-OCT images showed exudative signs, such as intraretinal and/or subretinal fluid, in 16/17 cases (94.1%).

At the last visit, OCTA images revealed that the mean total CNV area on OCTA choriocapillaris segmentation decreased to 1.31 ± 1.92 mm^2, with a mean vessel area of 0.71 ± 0.98 mm^2. Therefore, a decrease of 21.6% in total area and of 19.1% in vessel area was found on our overall cohort after anti-VEGF treatment.

In 6/17 (35.3%) cases, the pattern remained unchanged, corresponding to 2 medusas, 2 seafans, and 2 indistinct networks. In these six cases, patterns presented exudative signs on SD-OCT at final examination ($P = 0.034$). The main duration of follow-up of these 6 cases presenting constant patterns were 13.2 ± 4.1 months. These patients received an average of 7.5 ± 2.8 injections between both visits. Mean total

Table 2. Demographic and Clinical Features

Cases	Age (Years)	Sex	Naive or Treated State	CNV Type	Initial BCVA (Snellen)	Final BCVA (Snellen)	Exudative Signs at Baseline SD-OCT*	Exudative Status at Final SD-OCT*	No. of Injections at Baseline	No. of Injections During Follow-up	Follow-up Duration (Months)	Changers (Yes/No)†
1	83	M	Naive	1	20/25	20/20	+	−	0	6	11	Yes
2	85	M	Naive	2	20/64	20/25	+	−	0	6	9	Yes
3	86	F	Naive	2	CF	20/250	+	+	0	5	6	No
4	86	F	Naive	2	20/160	20/100	+	−	0	8	9	Yes
5	86	F	Treated	2	20/25	20/25	+	+	3	3	6	No
6	77	F	Naive	Mixed 1 and 2	20/25	20/20	+	+	0	8	10	Yes
7	73	F	Naive	Mixed 1 and 2	20/32	20/20	+	−	0	5	11	Yes
8	83	F	Treated	2	20/50	20/40	+	−	9	4	15	Yes
9	85	F	Treated	2	20/80	20/200	+	+	6	11	16	No
10	89	M	Naive	2	20/100	20/80	+	+	0	11	11	Yes
11	77	F	Treated	2	20/20	20/25	+	+	8	11	14	No
12	88	F	Treated	2	20/25	20/20	−	+	6	11	13	No
13	83	F	Naive	1	20/50	20/32	+	−	0	6	12	Yes
14	68	F	Naive	1	20/20	20/25	+	+	0	9	11	Yes
15	68	F	Treated	Mixed 1 and 2	20/32	20/25	+	+	9	8	11	Yes
16	80	M	Treated	1	20/25	20/40	+	−	21	6	17	Yes
17	80	M	Treated	1	20/25	20/20	+	+	5	6	17	No

*Exudative status at baseline and final SD-OCT examination refers to the presence or absence of intraretinal and/or subretinal fluid.

†Changers refer to the pattern between baseline and final follow-up visit of each patient. Patients marked with "Yes" correspond to the changing pattern group, whereas patients marked with "No" belong to the constant pattern group.

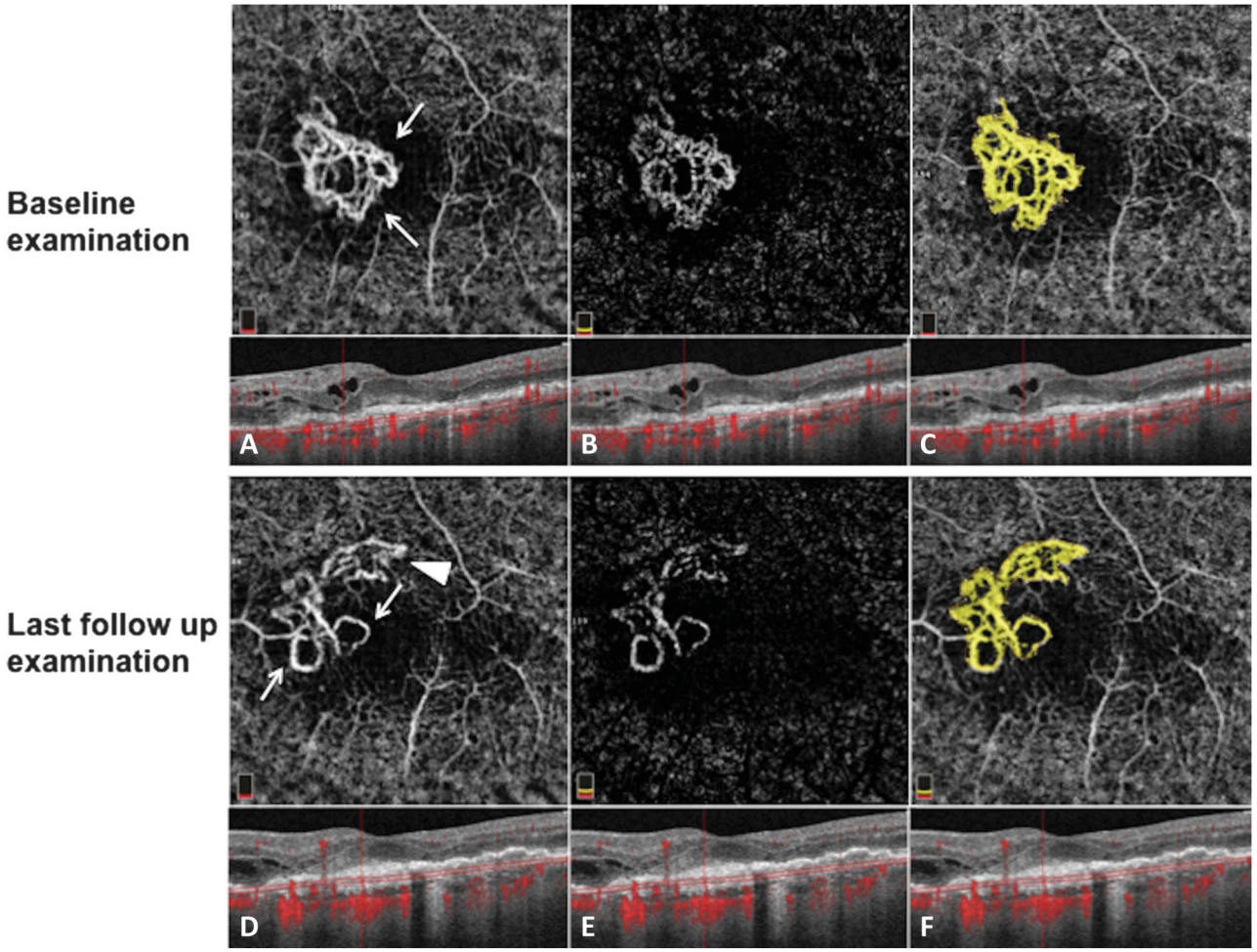

Fig. 2. Changes in CNV morphology from immature to mature pattern with persistence of exudative signs. Optical coherence tomography angiography imaging of an 86-year-old woman with an active Type 2 CNV at initial visit and 6 months later. The patient underwent 3 ranibizumab injections before baseline OCTA imaging and 3 other ranibizumab injections during the 6-month follow-up. Upper row (**A**, **B**, **C**) represents baseline visit OCTA flow images and corresponding B scans of the choriocapillaris segmentation (31–59 μm below the RPE). **A.** Reveals a high-flow network with a circumferential peripheral anastomosis (white arrows) and tiny capillary ramifications (thin branches) but no visualization of a feeder vessel. This criterion suggests that this high-flow network belongs to an "indistinct network" pattern. **B.** Corresponds to image (**A**) with projection artifact removal. **C.** The manual delineation and automatic measurement of the neovascular membrane: mean area at baseline averaged 0.58 mm^2. Lower row (**D**, **E**, **F**) represents the final follow-up visit OCTA flow images and corresponding B scans of the choriocapillaris segmentation. **D** and **E.** (with artifact removal) show the regression of tiny ramifications and persistance of the main vascular trunks with margin loops (white arrows). The enlarged caliber of the vessels is suggestive for arteriogenesis. Nonetheless, sprouting of new vessels can be observed in the superior part of the lesion (white arrowhead). **E.** The manual delineation and automatic measurement of lesion size. Mean area at follow-up was 0.65 mm^2, whereas at the baseline visit, mean area was 0.58 mm^2. Note that, while the mean area increased by 12.54%, vessel area diminished by only 4% (0.42 mm^2 at baseline vs. 0.40 mm^2 at the final visit).

area for the 6 eyes with constant pattern at final visit was 1.04 ± 0.95 mm^2, whereas mean vessel area was 0.61 ± 0.56 mm^2.

Conversely, at the last visit, the pattern changed on OCTA images in 11/17 (64.7%) eyes, revealing a pruned vascular tree pattern (Figures 1D and 2C), associated to flow void in 3 eyes. Final exudation was a variable, present in 4/11 (36.4%) eyes but absent in 7/11 eyes. In this group, the mean number of injections during the follow-up was 7.2 ± 2.5, during an average follow-up duration of 10.9 ± 2.7 months. Mean total area for the 11 eyes with changing pattern at final visit was 1.57 ± 2.68 mm^2, whereas vessel area averaged 0.82 ± 1.35 mm^2. Although the mean area at the final visit did not decrease in the "changing pattern" group (0.07%), it did decrease in the "constant pattern" group by 34.1% (1.04 mm^2 vs. 1.58 mm^2 at baseline). In terms of "vessel area," for the "changing pattern" group, we noted a mild decrease of 6.09%, whereas for the "constant pattern" group, we noted a decrease of 30.31%. No statistically significant difference was found between constant and changing pattern groups and final CNV area (P = 0.13 and P = 0.09, Mann–Whitney test).

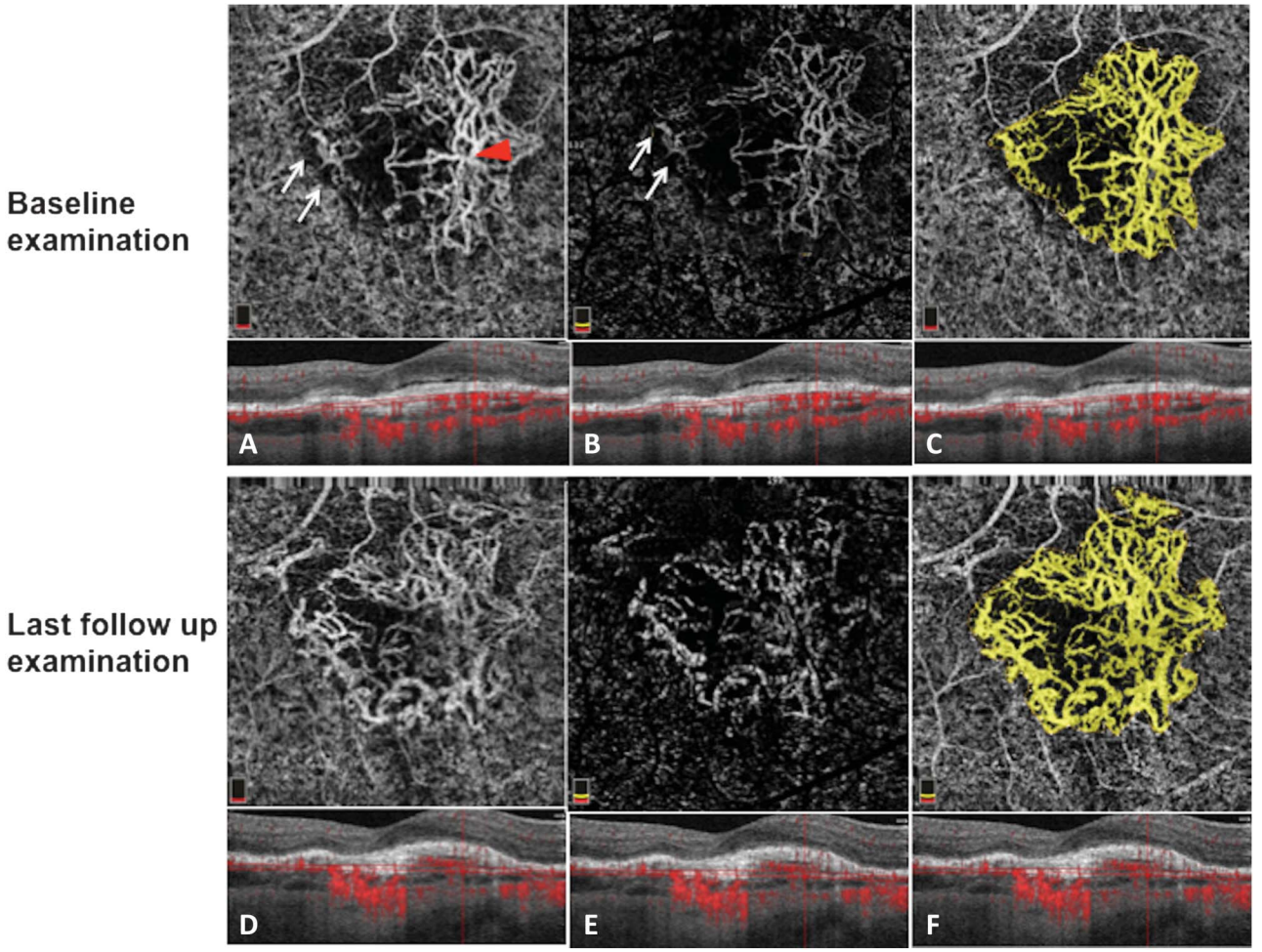

Fig. 3. Constant active pattern over time despite recurrent anti-VEGF treatment, associated with a persistent exudative activity in SD-OCT. Optical coherence tomography angiography imaging of an 83-year-old woman with a Type 2 CNV, previously treated by 9 anti-VEGF intravitreal injections at initial visit and 15 months later. The patient underwent four anti-VEGF injections between both examinations. Upper row (**A**, **B**, **C**) represents baseline visit OCTA flow images and corresponding B scans of the choriocapillaris segmentation. On (**A**), showing the unfiltered image, a central feeder vessel is visible (red arrow), together with a circular peripheral anastomosis, thin branches within and adjacent (white arrows) to the high-flow network, and a surrounding dark halo are present in the choriocapillaris segmentation. **B.** corresponds to image (**A**) with projection artifact removal. Note that the adjacent thin branches (white arrows), corresponding to capillary sprouting, are slightly less visible. **C.** The manual delineation and automatic measurement of the neovascular membrane. Mean area at baseline averaged 2.21 mm^2. Lower row (**D**, **E**, **F**) represents the final follow-up visit OCTA flow images and corresponding B scans of the choriocapillaris segmentation. **D** and **E.** (with artifact removal) show the persistence of thin branches and enlarged vascular trunks. **E.** Reveals the manual delineation and automatic measurement of the neovascular membrane. Mean area at final follow-up visit was 2.87 mm^2. Note that while the mean area increased by 23%, vessel area increased by only 29% (1.18 mm^2 at baseline vs. 1.66 mm^2 at the final visit).

Moreover, there was no significant difference in terms of initial and final BCVA between the "constant pattern" versus the "changing pattern" group ($P = 0.24$ and $P = 0.22$, respectively, Mann–Whitney test).

On the overall cohort, final OCTA images also revealed an increased caliber of main vascular trunks in 13/17 cases compared with the initial morphology. A dark halo was observed in 11/17 cases at initial examination (64.7%) and in 7/17 cases at final presentation (41.2%).

Treatment-Naive Versus Previously Treated Eyes

An additional analysis comparing treatment-naive and treated eyes in terms of pattern switching and area modifications was performed. Of the 9 treatment-naive eyes included in this study, 8 (88.88%) belonged to the "changing pattern" group at final follow-up visit. In terms of lesion area, a decrease in 21.34% of total area and 23.47% of vessel area was noted in these initially treatment-naive patients. Only one of nine treatment-naive eyes (11.11%) at baseline did not switch patterns after anti-VEGF therapy, being thus included in the "constant pattern" group. In this patient, the lesion area had increased by 15%, and vessel area increased by 2.3% at the final visit.

Of 8 previously treated eyes at study inclusion, 3 (37.5%) had changed patterns after anti-VEGF treatment, thus belonging to the "changing pattern" group

at the final examination, whereas 5/8 (62.5%) eyes had had a constant pattern throughout study period. In previously treated eyes belonging to the "changing pattern" group, there was an increase in 17.5% of total area and 1.33% of vessel area, respectively. On the contrary, treated eyes that had a constant pattern at final follow-up visit had a decrease in vessel area by 9.23%, whereas the vessel area decreased by 10%.

Interuser agreement for the qualitative variables, that is, neovascular patterns mentioned above was assessed using Cohen's Kappa coefficient. For the medusa pattern, Cohen's Kappa = 0.87 (standard error 0.24), for the seafan pattern, Cohen's Kappa = 0.82 (standard error = 0.24), whereas for indistinct network and pruned vascular tree pattern, Cohen's Kappa = 1 (standard error = 0.24), suggesting an almost perfect agreement between the 2 masked readers of the categorical variables used in this study. Interclass correlation was 0.99 for both total CNV area and vessel area, with a 95% confidence interval between 0.98 and 0.99.

Discussion

In our study, we aimed to describe long-term remodeling of CNV flow qualitatively and quantitatively in eyes undergoing anti–angiogenic therapy. Recent imaging studies have focused predominantly on short-term CNV flow remodeling when describing morphologic and quantitative changes of CNV flow in response to anti-VEGF treatment.[21–24] First of all, anti-VEGF therapy seems to induce a quantitative regression with a variable decrease in size and vessel density of the neovascular membrane, which has been described from 2 to 9.5 weeks after treatment.[9,21] A close OCTA monitoring between two anti-VEGF intravitreal injections has allowed other authors to confirm this "cyclic" flow remodeling hypothesis[23,24]: a pruning of smaller vessels occurred 24 hours after injection, increased and reached a maximum of flow regression between 6 days and 12 days, followed by a reproliferation (reopening or new sprouting of the vessels) 20 days to 50 days later.[24] Moreover, in a qualitative approach, Spaide depicted vascular "abnormalization" in treated CNV, called "arteriogenesis," characterized by the appearance of large-diameter vessels, loss of thin capillaries, and prominent anastomoses of vessels.[25] Furthermore, anti-VEGF treatment seems to be effective against newly formed capillaries from preexisting vascular trunks, a high VEGF dependent phenomenon called angiogenesis.[25]

In our study, OCTA images showed at baseline either the "medusa," "seafan," or "indistinct" pattern in all eyes included (17/17), with a mean total area of 1.58 ± 1.72 and 0.88 ± 0.95 mm^2 vessel area. At the final visit after anti-VEGF therapy, although there were slight, intrinsic changes in each high-flow CNV, the same flow pattern as at baseline was found in only 6/11 (35.3%) eyes, whereas 11/17 eyes (64.7%) of our series presented with morphologically different patterns.

Thus, by pooling baseline and final OCTA images and based on quantitative and qualitative data, our study identifies two types of progression of CNV morphology after anti-VEGF treatment: constant patterns, which conserve their rather disorganized morphology, with tiny capillaries and loops, are suggestive for immature CNV; changing patterns, however, are subject to arteriolization, with thicker, dilated vascular trunks and absence of tiny ramifications, ultimately suggestive for a mature neovascular lesion. Thus, morphologic changes within the CNV (and the corresponding "changing pattern" group) are evocative for the conversion from immature to mature features of the neovascular membrane.

Total area and vessel area were not correlated in a statistically significant manner with constant or changing pattern groups ($P = 0.13$ and $P = 0.09$, Mann–Whitney test). Although the neovascular membranes are immature, their response to anti-VEGF treatment can be translated into an important fluctuation in total and vessel areas, the two parameters being nonetheless proportional (34.1% decrease in total area vs. 30.31% decrease in vessel area); however, as the pattern changes and it matures, we notice a smaller variability of total area (0.07% decrease) and a larger decrease of vessel area (6.09%), correlated with anti-VEGF resistance in these patients.

Interestingly, when performing an additional analysis to see whether the changes (both morphologic and in size) were similar in treatment-naive and treated patients, 8 of 9 treatment-naive eyes had switched pattern over time, with a mean decrease in total area of 21.34%. Thus, the "changing pattern" group consisted majoritarily of initially naive eyes. This confirms our hypothesis on immature patterns having a higher fluctuation of total and vessel area in response to anti–angiogenic treatment. It is noteworthy to mention that most of the previously treated eyes included belonged at final visit in the "constant pattern" group (62.5%), with a modest decrease of mean area and vessel area (9.23 and 10%, respectively). Total area, although not being correlated to CNV activity, is in fact correlated with the immaturity or maturity of the neovascular membrane. Moreover, these findings also suggest that vessel area could provide important information on the therapeutic response to anti-VEGF.

In this study, there was no statistically significant correlation between one group and changes in the

neovascular membrane total area and vessel area, probably because of our small sample size. However, constant patterns over time (immature) had a higher vessel area and were correlated in a statistically significant manner with exudative signs on SD-OCT imaging ($P = 0.034$). However, exudation on SD-OCT was present in CNV patterns classified as mature in 36.4% cases, suggesting that, even when the tiny ramifications corresponding to neoformed capillaries disappear, mature, large vascular trunks within CNV may generate exudative features on SD-OCT. Moreover, Ichiyama et al[26] have recently demonstrated that better functional outcomes were correlated with an increased vascularity of the CNV, thus an increased vessel area, in eyes that had not been treated by anti-VEGF in more than 6 months. Consequently, there are still many unknown variables in the relationship between anatomical and functional outcomes after anti-VEGF therapy.

Additional morphologic changes at the final visit, such as signal voids, were observed at the final visit in 3/17 cases, all of which belonged to the changing pattern group. Absence of CNV visualization in OCTA was previously associated with clinical and SD-OCT exudative inactivity.[18,27] Nonetheless, the absence of CNV visualization in the choriocapillaris segmentation may be due to other reasons, such as the masking effect generated by a high PED, media opacities, or the presence of hemorrhages.[28]

The limits of our study are related to technical limitations of OCTA technology. Our small sample size and the heterogeneous nature (treatment-naive and treated eyes) of our cohort, with variable follow-up durations, are also among the limitations of this study. Moreover, we used the instrument's automated segmentation for image analysis and quantitative measurements, regardless of the particularities in segmenting mixed and Type 2 CNV. The automated segmentation may also explain, in part, the good intergrader agreement obtained. Concerning OCTA limitations, projection, motion, and image processing artifacts are still an important issue in current OCTA technology, which can essentially alter image interpretation.[28]

In conclusion, this study reveals flow remodeling occurring with anti-VEGF treatment in neovascular AMD patients. Indeed, the initial CNV pattern observed frequently switched toward a mature pattern after anti-VEGF therapy. Despite the complexity of vascular phenomena involved in neovascular recurrence and remission,[29] OCTA suggests that there is a strong correlation between the morphology (and not the size) of CNV and their structural response (or lack thereof) to treatment. Optical coherence tomography angiography thus highlights the strengths and weaknesses of current therapies, helping to understand the pathophysiological implications of neovascular AMD and to monitor disease progression in treated eyes.

Key words: anti–vascular endothelial growth factor, choroidal neovascularization, age-related macular degeneration, flow remodeling, high-flow network, optical coherence tomography angiography.

References

1. Ferris FL, Fine SL, Hyman L. Age-related macular degeneration and blindness due to neovascular maculopathy. Arch Ophthalmol 1984;102:1640–1642.
2. Wong TY, Wong T, Chakravarthy U, et al. The natural history and prognosis of neovascular age-related macular degeneration: a systematic review of the literature and meta-analysis. Ophthalmology 2008;115:116–126.
3. Freund KB, Zweifel SA, Engelbert M. Do we need a new classification for choroidal neovascularization in age-related macular degeneration? Retina 2010;30:1333–1349.
4. Schachat AP. Management of subfoveal choroidal neovascularization. Arch Ophthalmol 1991;109:1217–1218.
5. Stanga PE, Lim JI, Hamilton P. Indocyanine green angiography in chorioretinal diseases: indications and interpretation: an evidence-based update. Ophthalmology 2003;110:15–21.
6. Sulzbacher F, Kiss C, Munk M, et al. Diagnostic evaluation of type 2 (classic) choroidal neovascularization: optical coherence tomography, indocyanine green angiography, and fluorescein angiography. Am J Ophthalmol 2011;152:799–806.
7. Freund KB, Ho IV, Barbazetto IA, et al. Type 3 neovascularization: the expanded spectrum of retinal angiomatous proliferation. Retina 2008;28:201–211.
8. Yannuzzi LA, Freund KB, Takahashi BS. Review of retinal angiomatous proliferation or type 3 neovascularization. Retina 2008;28:375–384.
9. Yannuzzi LA, Negrão S, Iida T, et al. Retinal angiomatous proliferation in age-related macular degeneration. Retina 2001;21:416–434.
10. López-Sáez MP, Ordoqui E, Tornero P, et al. Fluorescein-induced allergic reaction. Ann Allergy Asthma Immunol 1998;81:428–430.
11. Giovannini A, Amato GP, Mariotti C, et al. OCT imaging of choroidal neovascularisation and its role in the determination of patients' eligibility for surgery. Br J Ophthalmol 1999;83:438–442.
12. Kim DY, Fingler J, Zawadzki RJ, et al. Optical imaging of the chorioretinal vasculature in the living human eye. Proc Natl Acad Sci U S A 2013;110:14354–14359.
13. Choi W, Mohler KJ, Potsaid B, et al. Choriocapillaris and choroidal microvasculature imaging with ultrahigh speed OCT angiography. PLoS One 2013;8:e81499.
14. Schwartz DM, Fingler J, Kim DY, et al. Phase-variance optical coherence tomography: a technique for noninvasive angiography. Ophthalmology 2014;121:180–187.
15. Kuehlewein L, Bansal M, Lenis TL, et al. Optical coherence tomography angiography of type 1 neovascularization in age-related macular degeneration. Am J Ophthalmol 2015;160:739–748.
16. El Ameen A, Cohen SY, Semoun O, et al. Type 2 neovascularization secondary to age-related macular degeneration imaged

by optical coherence tomography angiography. Retina 2015; 35:2212–2218.
17. Miere A, Querques G, Semoun O, et al. Optical coherence tomography angiography in early type 3 neovascularization. Retina 2015;35:2236–2241.
18. Miere A, Semoun O, Cohen SY, et al. Optical coherence tomography angiography features of subretinal fibrosis in age-related macular degeneration. Retina 2015;35:2275–2284.
19. Bird AC, Bressler NM, Bressler SB, et al. An international classification and grading system for age-related maculopathy and age-related macular degeneration. The International ARM Epidemiological Study Group. Surv Ophthalmol 1995;39:367–374.
20. Coscas GJ, Lupidi M, Coscas F, et al. Optical coherence tomography angiography versus traditional multimodal imaging in assessing the activity of exudative age-related macular degeneration : a new diagnostic challenge. Retina 2015;35: 2219–2228.
21. Muakkassa NW, Chin AT, de Carlo T, et al. Characterizing the effect of anti-vascular endothelial growth factor therapy on treatment-naive choroidal neovascularization using optical coherence tomography angiography. Retina 2015;35:2252–2259.
22. Kuehlewein L, Sadda SR, Sarraf D. OCT angiography and sequential quantitative analysis of type 2 neovascularization after ranibizumab therapy. Eye Lond Engl 2015;29:932–935.
23. Marques JP, Costa JF, Marques M, et al. Sequential morphological changes in the CNV net after intravitreal anti-VEGF evaluated with OCT Angiography. Ophthalmic Res 2016;55: 145–151.
24. Lumbroso B, Rispoli M, Savastano MC, et al. Optical coherence tomography angiography study of choroidal neovascularization early response after treatment. Dev Ophthalmol 2016; 56:77–85.
25. Spaide RF. Optical coherence tomography angiography signs of vascular abnormalization with antiangiogenic therapy for choroidal neovascularization. Am J Ophthalmol 2015; 160:6–16.
26. Ichiyama Y, Sawada T, Ito Y, et al. Optical coherence tomography angiography reveals blood flow in choroidal neovascular membrane in remission phase of neovascular age-related macular degeneration. Retina 2017;37:724–730.
27. Liang MC, de Carlo TE, Baumal CR, et al. Correlation of spectral domain optical coherence tomography angiography and clinical activity in neovascular age-related macular degeneration. Retina 2016;36:2265–2273.
28. Spaide RF, Fujimoto JG, Waheed NK. Image artifacts in optical coherence tomography angiography. Retina 2015;35:2163–2180.
29. Spaide RF. Choroidal neovascularization. Retina 2017;37: 609–610.